

# Breaking the Frame: Visual Place Recognition by Overlap Prediction

Tong Wei<sup>1</sup>  
weitong@fel.cvut.cz

Philipp Lindenberger<sup>2</sup>  
philipp.lindenberger@inf.ethz.ch

Jiří Matas<sup>1</sup>  
matas@fel.cvut.cz

Daniel Barath<sup>2</sup>  
danielbela.barath@inf.ethz.ch

<sup>1</sup> Visual Recognition Group, FEE, Czech Technical University in Prague

<sup>2</sup> Computer Vision and Geometry Group, ETH Zurich

## Abstract

Visual place recognition methods struggle with occlusions and partial visual overlaps. We propose a novel visual place recognition approach based on overlap prediction, called VOP, shifting from traditional reliance on global image similarities and local features to image overlap prediction. VOP proceeds co-visible image sections by obtaining patch-level embeddings using a Vision Transformer backbone and establishing patch-to-patch correspondences without requiring expensive feature detection and matching. Our approach uses a voting mechanism to assess overlap scores for potential database images. It provides a nuanced image retrieval metric in challenging scenarios. Experimental results show that VOP leads to more accurate relative pose estimation and localization results on the retrieved image pairs than state-of-the-art baselines on a number of large-scale, real-world indoor and outdoor benchmarks. The code is available at <https://github.com/weitong8591/vop.git>.

## 1. Introduction

Visual Place Recognition (VPR) is defined as the task of identifying the approximate location where a query image was taken, given a certain tolerance level [2, 7, 14, 19–21, 23, 26, 30, 55, 56, 58, 60]. VPR methods have been widely used in computer vision and robotics [10, 12] problems, such as autonomous, unmanned aerial [32], terrestrial, and underwater vehicles [43], as well as recent AR/VR devices.

Typically, VPR is approached as an image retrieval problem, where the image to be localized is compared against a large database of posed images and, optionally, a 3D re-

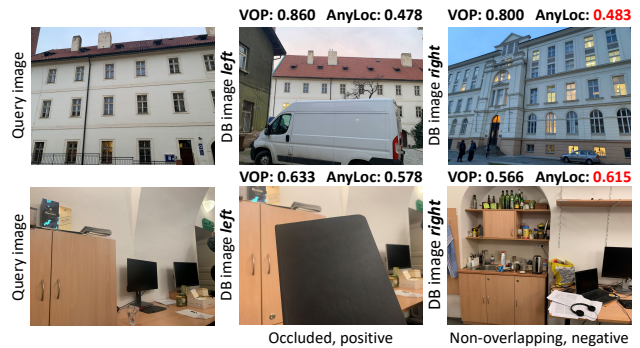


Figure 1. An example where the SOTA AnyLoc [25] scores a negative DB image (right, at a different location) higher than an occluded positive example (left, the same scene as the query with heavy occlusion). VOP ranks the database (DB) images correctly.

construction of the scene. Then, the most similar images retrieved from the database are used to estimate the precise location of the input query image, e.g., via local feature detection and matching. The complexity of VPR stems from a variety of factors such as seasonal variations, changes in viewpoint, the presence of dynamic objects, illumination differences, occlusions, weather conditions, and large-scale environments, as discussed in the studies by Hong *et al.* [22], Doan *et al.* [15], and Subramaniam *et al.* [50].

Recent approaches implement VPR as an estimation of image similarity and retrieval through learned image embeddings generated by a feature extraction architecture augmented with an aggregation or pooling mechanism, such as NetVLAD [2], CosPlace [6], and AnyLoc [25]. In such frameworks, images from the database are retrieved by optimizing their similarity between the embeddings to the

query image, *e.g.*, cosine similarity. One notable drawback of these methods is their sensitivity to partial overlaps resulting from occlusions. In practice, occlusions can significantly reduce image similarity scores despite the unobstructed portions of the scene, potentially offering valuable cues for localization. Second, such methods optimize the similarity of the embeddings on positives closer than the negative samples, which is hard to train as there is no ground truth (GT) prior to indicating the exact degree of similarity. Instead, we build GT patch matches as supervised by the 3D reconstruction. In addition, several reranking-based VPR methods [20, 62] retrieve the most similar images from the database on the shortlist built by global embeddings. Those improves the performance of retrieving correct images but needs more storage .

Instead of relying on global similarities or local features, we frame the problem as overlap prediction. This enables us to methodically understand which parts of a particular image are visible without having to perform feature detection and matching. Also, focusing on overlaps makes VOP more robust to occlusions and provides a better understanding of the query image in relation to the database. VOP encodes individual patches rather than the entire image, thereby facilitating the efficient establishment of patch-to-patch correspondences. These matches are subsequently utilized within a voting mechanism to calculate an overlap score for potential database images, providing a nuanced metric for retrieval amidst complex visual environments.

In Fig. 1, we show two retrieval examples using the proposed Visual Place Recognition by Overlap Prediction (VOP) and AnyLoc [25], a state-of-the-art retrieval solution. They process a query image alongside two database images: one sharing the scene with the query albeit with occlusion, and another from a different environment. AnyLoc erroneously attributes higher similarity to the unrelated image. In contrast, our proposed approach successfully identifies the correct image and the areas likely to overlap.

The contributions of this paper are as follows:

1. A novel approach focusing on patch overlap assessment, exhibiting enhanced robustness to challenges such as occlusions. The proposed method, **VOP**, learns patch embeddings suitable for visual localization and implements a single radius search across image patches in the database.
2. The introduction of a robust voting mechanism for image retrieval shows improvement over conventional similarity-based methods with nearest neighbors.
3. Breaking the frame of looking for close database images in standard VPR methods by considering geometric applications and using specific evaluation metrics.

## 2. Related Work

Image retrieval methods for VPR problems can be categorized into two groups, one globally representing the whole image and the other locally for keypoints using hand-crafted or learning-based embeddings.

**Place recognition** is often cast as an image retrieval problem [2, 6, 7, 18, 20, 23, 25, 27, 37, 38, 58] that consists of two phases. In the offline indexing phase, a reference map represented by an image database is created. In the online retrieval phase, a query image, taken during a later traverse of the environment, is coarsely localized by identifying its closest matches within the reference map.

To find the closest matches in the indexing structures, traditional methods like Bag of Visual Words [11] (BoW) identify key local image patches and store them as a codebook. BoW is often used in conjunction with 128-dimensional SIFT [31] descriptors both for map creation and image retrieval. These high-dimensional features often require approximate nearest neighbor (NN) search or GPUs to accelerate the searching process. Showcasing the unbroken popularity of such approaches, they are still widely employed in applications, *e.g.*, in ORB-SLAM [9, 33, 34].

As demonstrated by Zheng *et al.* [61], using CNNs to improve hand-crafted features in various applications, namely through compact (fixed-length) representations, has gradually become the norm. Most recent methods utilize learned embeddings generated by a feature extraction backbone with an aggregation or pooling head, *e.g.*, NetVLAD [2]. In recent works, transformer-based retrieval methods [16] have been introduced, incorporating metric learning and attention mechanisms. These methods utilize local and global features, or a fusion of the two, to identify similar images.

**Global retrieval methods** usually integrate or combine handcrafted or learning-based local descriptors, such as SIFT [31] through the BOW model [39, 48], or employ alternative algorithms [54]. There is a growing trend towards learning-based techniques that devise improved methods for feature aggregation. NetVLAD [2] introduces an end-to-end trainable image representation extractor, employing weak supervision through soft assignment to cluster centers. Generalized Mean Pooling (GeM) [40] proposes a learnable pooling layer that generalizes both max and average pooling, with a CNN serving as the backbone. Additionally, AP-GeM [42] enhances ranking accuracy by minimizing a relaxed global mean Average Precision (mAP) over a set of images. A CNN-based solution, CosPlace [6], utilizes the CNN backbone and GeM pooling but approaches the place retrieval issue as a classification problem. MixVPR [1] transitions feature maps into a compact representation space through cascade MLP blocks. AnyLoc [25] emerges as a versatile method suitable for various image retrieval contexts, exploring CNN-based or Vision Transformer (ViT)-

based foundational models and aggregation techniques to construct a vocabulary for searching in a large database. More recently, DINOv2-SALAD [24] finetunes DINOv2 and proposes a new aggregation method based on optimal transport and the relations between features and clusters.

**Image reranking.** Visual place recognition techniques have increasingly embraced a two-phase approach that pairs global retrieval with subsequent reranking based on local features. MultiVLAD [3] is proposed to use the maximum similarity between the query VLAD descriptors and the query as the matching score. Similarly, Razavian. *et al.* [47] rely on the average L2 distance of each query sub-patch to the reference image. Patch-NetVLAD [20], for instance, innovates by integrating NetVLAD with region-level descriptors and multi-scale patch tokens for enhanced geometric verification. It effectively merges the strengths of local and global descriptors, offering high resilience to changes in condition and viewpoint. RRT [52] and TransVPR [57] further this development by incorporating image-level supervision and attention-based mechanisms, respectively, focusing on spatial relationships and feature relevance within images. CVNet and  $R^2$ Former [62] introduce methodologies for replacing traditional geometric verification with dense feature correlation and transformer-based reranking, focusing on the precise alignment of features and relevance of image pairs. SuperGlobal [46] simplifies the reranking process by relying on global features and K-nearest-neighbors aggregation, showcasing a move towards more scalable and computationally efficient VPR solutions. These advancements highlight a trend toward utilizing machine learning techniques, including deep learning and transformers, to refine the accuracy and efficiency of image retrieval.

### 3. Visual Overlap Prediction (VOP)

In this section, we describe the method proposed for efficiently predicting visual overlap in large image collections.

#### 3.1. Problem Statement

In place recognition problems, the aim is to find images  $I_j \in \mathbb{R}^{H \times W \times C}$  containing the same landmark or scene as the query  $I_i \in \mathbb{R}^{H \times W \times C}$ . Usually, it is done by transforming the images to a high-dimensional embedding space and measuring the distances to select the top- $k$  most similar images. In this embedding space, an image  $I_i$  is represented by a high-dimensional global  $\mathbf{g}_i \in \mathbb{R}^{d_g}$  or local descriptors  $\mathbf{d}_i \in \mathbb{R}^{n_l \times d_l}$ , using encoder  $f(\cdot)$ , where  $n_l \in \mathbb{N}$  denotes the number of local features, with the dimensions  $d_g \in \mathbb{N}$ ,  $d_l \in \mathbb{N}$ . The matching score, then, can be computed as the similarities of the descriptors,  $s(I_i, I_j) = \text{sim}(\mathbf{d}_i, \mathbf{d}_j)$  or  $\text{sim}(\mathbf{g}_i, \mathbf{g}_j)$ , for example, as their cosine similarity.

Local features are usually image-dependent and redundant with variable lengths. Instead, we focus on patch-level

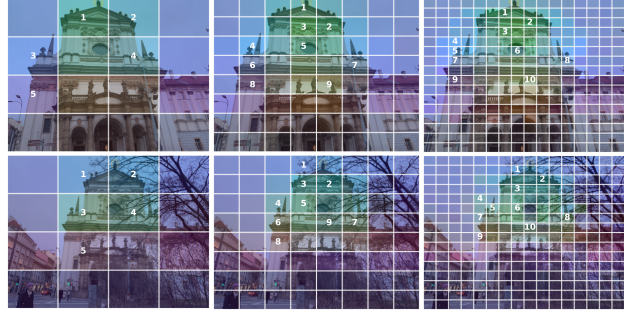


Figure 2. Patch matching examples in an image pair (column) with varying patch sizes (16, 64, and 256). The 256 patches from DINOv2 [35] are average pooled to 16 and 64 patches. In each column, the numbers inside the patches indicate which ones are matched. The color overlay is calculated by applying PCA to the patch embeddings.

representations and redefine the matching score as the overlap between the images. It is simple and efficient to achieve patch-level descriptors with less dependency. Let us split image  $I$  into a set  $\mathcal{P}$  of rectangular patches by a uniform grid consisting of  $n$  rows and columns. Given sets of such rectangular patches  $\mathcal{P}_i$  and  $\mathcal{P}_j$  in the two images, there are multiple ways to define overlap. Here we define a patch-level overlap score as follows:

$$o(p, q) = \text{volume}(\text{cone}(\mathbf{R}_i, \mathbf{t}_i, \mathbf{K}_i, p), \text{cone}(\mathbf{R}_j, \mathbf{t}_j, \mathbf{K}_j, q)), \quad (1)$$

for each pair  $(p, q)$ , where  $p \in \mathcal{P}_i$  and  $q \in \mathcal{P}_j$  are the image patches,  $\mathbf{R} \in \text{SO}(3)$  are the absolute rotations of the cameras,  $\mathbf{t} \in \mathbb{R}^3$  are absolute positions,  $\mathbf{K} \in \mathbb{R}^{3 \times 3}$  represents the intrinsic camera parameters, function  $\text{cone}(\cdot)$  is the 3D cone defined by the camera pose and the current patch, function  $\text{volume}(\cdot, \cdot)$  measures the overlap of two posed cones in three dimensions. While this measure is easy to calculate given the camera poses and intrinsics, we observed that it does not reflect real-world applications, *e.g.*, 3D reconstruction. Thus, we reformulate this measure as follows:

$$o'(p, q) = \sum_{X \in \mathcal{X}} [\text{inside}(\mathbf{K}_i(\mathbf{R}_i \mathbf{X} + \mathbf{t}_i), p)] * [\text{inside}(\mathbf{K}_j(\mathbf{R}_j \mathbf{X} + \mathbf{t}_j), q)], \quad (2)$$

where  $\mathcal{X} \subset \mathbb{R}^3$  comprises 3D points from a 3D reconstruction of the environment, formula  $\mathbf{K}(\mathbf{R} \mathbf{X} + \mathbf{t})$  projects a 3D point to the image, function  $\text{inside}(\cdot)$  checks whether a 2D point falls into a 2D patch,  $[\cdot]$  is the Iverson bracket which equals one if the condition inside holds and zero otherwise.

Eq. 2 defines the patch overlap as the number of 3D points commonly visible on both patches. Then the overlap of two entire images  $I_i$  and  $I_j$  is defined as the sum of

overlap scores across matching patches as follows:

$$O(I_i, I_j) = \sum_{p \in \mathcal{P}_i} \sum_{q \in \mathcal{P}_j} o'(p, q) = \sum_{(p, q) \in \mathcal{C}} o'(p, q), \quad (3)$$

where set  $\mathcal{C} = \{(p, q) \mid p \in \mathcal{P}_i, q = \arg_w \max o'(p, w) \in \mathcal{P}_j, w \in \mathcal{P}_j\}$  is a set of patch-to-patch correspondences defined by assigning the most similar patch from the database image to each patch in the query.

However, this formulation still does not allow for retrieval, as the camera pose corresponding to the query image is unknown in practice. Thus, we further approximate the image overlap as the similarities between the patch embeddings in a robust way as follows:

$$\hat{O}(I_i, I_j) = \sum_{(p, q) \in \mathcal{C}} \rho(\text{sim}(f(p), f(q))), \quad (4)$$

where  $f(\cdot)$  is an encoder with a single patch as input, usually using deep networks or hand-crafted methods, and  $\rho: \mathbb{R} \rightarrow \mathbb{R}$  is a robust function, e.g.,  $\rho$  can be defined as a voting mechanism as  $\rho(x) = \llbracket x > \epsilon \rrbracket$ , where  $\epsilon$  is a manually set threshold with  $x$  as the patch similarity  $\text{sim}(f(p), f(q))$ .

Given such a scheme to quantify image overlap via the similarity of a set of patch correspondences, the most similar image  $I^*$  that we retrieve for query  $I_i$  from a set of database images  $\{I_j\}, j \in 1, \dots, N$  is the one with the highest overlap, calculated as follows:

$$I^* = \arg_{j \in 1, \dots, N} \max \hat{O}(I_i, I_j). \quad (5)$$

In the scenario where multiple images need to be retrieved for a single query, we straightforwardly define a ranking by sorting images with high visual overlap. Thus, image retrieval from collections becomes a patch-matching problem. Example matches are visualized in Fig. 2. Next, we will talk about how to learn the encoder  $f(\cdot)$  in VOP focusing on accurate overlap prediction.

### 3.2. Learning Patch Matching via Patch Similarities

In order to find the similarity of image patches  $p$  and  $q$  in images  $I_i$  and  $I_j$ , respectively, we aim to learn an embedding  $f(\cdot)$  that allows for casting the problem as a descriptor matching. Thus, we aim to distill embeddings  $e_p \in \mathbb{R}^d$  and  $e_q \in \mathbb{R}^d$  such that  $\text{sim}(p, q) (= \delta(e_p, e_q) = \delta(f(p), f(q)))$  is high if and only if  $p$  and  $q$  are overlapping and zero otherwise. The function  $\delta(\cdot)$  measures the similarity in the embedding space, e.g., as the cosine similarity.

The **pipeline** for learning patch-level embeddings is visualized in Fig. 3. Given a pair of images  $I_i$  and  $I_j$ , the problem is to learn embeddings  $e_p$  and  $e_q$  as defined previously. First, we obtain patch features by inputting the images into a Visual Transformer architecture. We use a frozen DINOv2 [35] backbone. These features are then fed

into an encoder head, comprising one linear projection layer plus a few fully connected layers with GELU activation and a dropout layer to encode the centers of the patches. Given the corresponding patch pair  $(p, q)$  as a positive sample, we train this encoder to predict similar embeddings for  $p$  and  $q$ . To do so, we employ contrastive learning on the similarities over the trained embeddings.

**Contrastive Learning.** We use contrastive learning to learn a joint embedding space for the image patches. To do so, we form patch pairs  $(p, q)$ . Real-world scenes are rarely static, e.g., objects move or undergo non-rigid deformations and illumination changes. To ensure that the learned embedding is robust to such temporal changes, we use image augmentation techniques as implemented in GlueFactory [29], such as adding random brightness, blur, flip, and noise.

For each query patch  $p$ , we prepared a set of candidate patches  $\{q, q_1, q_2, \dots, q_n\}$  for training, where  $\{q_1, q_2, \dots, q_n\}$  act as  $n$  negative samples, depicting patches that do not have a common field-of-view with the query patch. In our training pipeline, half of the samples have no overlap (negative samples), e.g., they depict different scenes. The other half are from the same scene as the query. In the samples, there are 30-90% negative patches, which are the ones not matchable with the query patch. We consider the loss in a patch-level manner. We train our model by optimizing the contrastive loss on the similarities of the embeddings. The contrastive loss on patch-to-patch matching pairs is defined as:

$$\mathcal{L}_{\text{contrastive}} = \frac{1}{n^2} \sum_i^n \sum_j^n \left( l_{\text{GT}} * (\sigma - \delta(e_p, e_q))^2 - (1 - l_{\text{GT}}) * \delta(e_p, e_q)^2 \right), \quad (6)$$

where  $l_{\text{GT}}$  is the ground-truth labels for each pair of patches (one from the query image and the other from the database). It is positive if their similarity is larger than a threshold  $\llbracket \text{sim}(p_i, q_j) > \epsilon \rrbracket$  and vice visa. Parameter  $\delta(\cdot)$  is the similarity measurement of the  $d$ -dimensional descriptors, i.e., cosine similarity with  $\sigma = 1$  as the margin. It penalizes the cases of high similarities on the patches but non-overlapping in the ground truth, i.e., no visible 3D points. We resize the input images to a fixed size. Therefore, the overall loss is averaged over  $n^2$  tentative matching patches on one image pair. We also experimented with incorporating attentions into the procedure. However, we noticed that the attention layers only increase the size of the network while leading to worse generalization performance. Thus, we keep only the contrastive loss for training.

To provide means for quick prefiltering, we add a classification ([CLS]) token to the employed Transformer network that is trained to distill global image embeddings based on the image overlap scores, shown in the ablations.

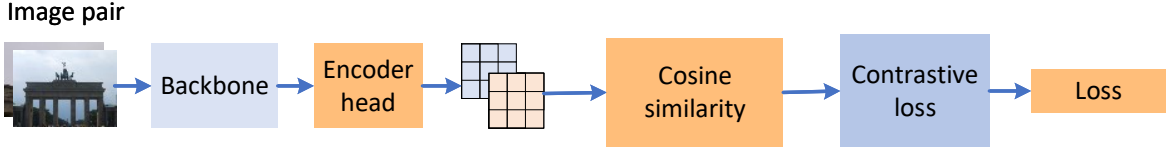


Figure 3. The learning pipeline of the proposed Visual Overall Prediction (VOP) method is shown, with a frozen ViT backbone [35], trainable encoder head, and contrastive loss on the similarities. The input to the training is image pairs that are broken down into rectangular patches to learn patch-to-patch overlap scores.

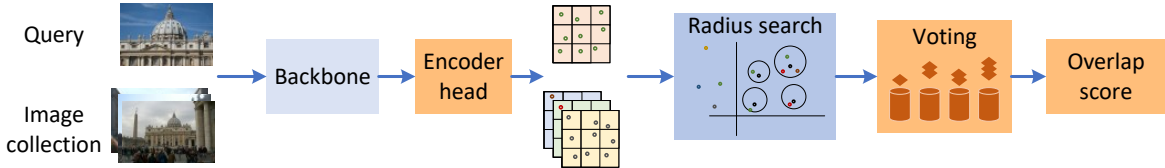


Figure 4. The proposed Visual Overlap Prediction (VOP) method at inference. Given an input query image and an image collection representing the reference map, the images are broken down into rectangular patches, the frozen backbone [35] extracts patch-level features, which are then fed into an encoder network, obtaining the final embeddings. The image retrieval is performed by running a radius search in the embedding space for each query patch to find potential database matches. The final overlap scores are determined by robust voting on the formed “query patch”-to-“database patch” correspondences. In practice, the map embeddings are obtained in an offline.

These tokens are used to efficiently select a subset of potentially overlapping images given the query.

**Constructing Training Data.** Now, we introduce the visual supervision used to build GT labels for training. The ground-truth overlapping patches of the training image pairs are achieved following LightGlue [29] employing pixel-wise depth and relative pose. As shown in Eq. 2, the patch overlap is measured by counting the co-visible 3D points in the reconstruction. The ground-truth matching local patches are found in two steps: First, a set of dense pixel coordinates  $c_i$  are detected in the first image  $I_i$ , and transformed to 3D points  $X_i$ . The obtained 3D point cloud is filtered by non-zero depths and transformed to the reference camera, *i.e.*, projecting the keypoints from camera  $i$  to  $j$  by the given transformation matrix,  $kp_{i2j}$ . Given camera intrinsics, we project the 3D points  $X_i$  to the camera planes and check for visibility. We make sure that only cycle-consistent points are kept by using the projected point, calculating its 3D coordinates, and back-projecting to the original image for a visibility check again. The ground-truth matches are supposed to contain the points with a consistent depth [29]. This procedure provides the initial set of positive and negative pairs of matching image patches.

Next, given the visible pixel matches, we check which patches they belong to and define the matchable patches by having at least one visible pixel correspondence. We assume one-to-one matching relations, *i.e.*, the patch with the most patch matches in the image pair will be chosen if there are multiple. Note that the visual supervision is built mutually from the image to the reference and vice versa.

### 3.3. Image Retrieval by Overlap Scores

Given a query image  $I_i$  and a set of database images  $I_{j=1,\dots,N}$ , our goal is to efficiently determine the top- $k$  images for  $I_i$  maximizing overlap. To do so, in the offline mapping phase of the method, we pre-generate the patch embeddings of all images in the database.

The retrieval pipeline is visualized in Fig. 4. In the on-line phase, we obtain the patch and, optionally, the global embeddings of the query image. Next, for each query image patch, we perform a radius search in the database of patch embeddings to determine all potentially overlapping candidates. Setting a radius threshold  $\epsilon$  is easy as the employed cosine similarity falls between 0 and 1. We tune this threshold on the validation set and use a fixed one in all our experiments. Note that k-nearest-neighbors algorithm is insufficient in our case as we would like to find all potentially overlapping patches to determine image overlaps. Such a radius search can be efficiently performed by standard bounding structures, *e.g.*, kd-tree, and other implementation tricks. Optionally, we also use the global descriptor to prefilter the images to a shortlist.

To obtain the top- $k$  images, we perform voting such that the overlap calculation becomes:

$$\hat{O}(I_i, I_j) = \sum_{(p,q) \in \mathcal{C}} \llbracket sim(p, q) > \epsilon \rrbracket, \quad (7)$$

quantifying the image overlap as the count of overlapping patches inside the images, or the sum of the similarities of

the descriptors as

$$\hat{O}(I_i, I_j) = \sum_{(p,q) \in \mathcal{C}} \max(\delta(e_p, e_q) - \epsilon, 0). \quad (8)$$

**Weighted Voting.** To highlight the distinguishable query patches, we propose to weight the query patches from each image using a bag of visual words approach [11]. Specifically, we apply TF-IDF [41] weights to all the query patches, assigning lower weights to patches that frequently appear in queries but are rare in the matched database patches. As illustrated below, it is preferable to have more neighbor patches if fewer images share the same neighborhood with the query patch. For each query patch, the weight  $t_i$  is calculated as follows:

$$t_i = \frac{n_{id}}{n_d} \log \frac{N}{n_i}, \quad (9)$$

where  $n_{id}$  is the number of neighbor patches in database images, defined as the cosine similarities of the patch descriptors within a specified radius, and  $n_d$  is the total number of patches in each image, *i.e.*, 256 in our case, with a patch size of (14, 14) on the resized image size of 224. Parameter  $N$  represents the total number of database images, and  $n_i$  denotes the number of database images that contain at least one neighbor of the query patch. Patches that frequently appear are deemed less important and thus are down-weighted. Weight  $t_i$  for each query patch is incorporated into the overlap score computation as follows:  $t_i * \hat{O}(I_i, I_j)$ . Note that the map weights are precomputed during the mapping phase.

## 4. Experimental Results

Our experiments include estimating two-view epipolar geometry and localizing query images from retrieved images. The VOP model is trained on 153 scenes from the MegaDepth dataset [28], which includes Internet-sourced images and depths reconstructed via Structure-from-Motion (SfM) and multi-view stereo techniques. Beyond the MegaDepth testing scenes, we evaluate the generalization ability of the proposed VOP on 11 scenes from Photo-Tourism [49], 13 scenes from ETH3D [45], and the InLoc dataset [51]. We benchmark the proposed method against several competitors, including the DINOv2, CNN-based retrieval methods like NetVLAD [2] and CosPlace [6], as well as the state-of-the-art (SOTA) retrieval method AnyLoc [25] and DINOv2-SALAD [24] utilizing the same DINOv2 backbone as VOP. Besides those *global-only* methods, we compare **VOP** with the SOTA reranking-based methods: the ViT-based  $R^2$ Former [62] and the CNN-based Patch-NetVLAD [20]. Also, we finetune Cosplace\* on the same dataset our method was trained on to demonstrate that

the improved performance is not due to the different training data. In addition, we test reranking methods [20] [62] on the shortlists created by DINOv2 [CLS] token, similarly as done for VOP, marked with † in the tables.

**Training Details.** The models underwent training on the 153 MegaDepth scenes, employing contrastive loss to differentiate negative and positive patch pairs. Each scene contributes 150 positive and 150 negative image pairs to the training set, standardized to an image resolution of  $224 \times 224$  pixels. We use the DINOv2 pre-trained model with a patch size of 14 to extract 1024-dimensional descriptors and reduce them to 256 dimensions by a fully-connected layer, *i.e.*, the first layer of our training encoder head. Negative images, characterized by zero overlaps (*e.g.*, sourced from distinct scenes), contrast with positive samples randomly selected from the pairs with 10% to 70% overlapping patches. Notably, the contrastive loss framework is predicated on patch-level negative/positive distinctions rather than entire images. Note that cosine similarity is used in the contrastive loss. Following LightGlue [29], patch-level labels are generated from depth information and visual features, utilizing the GlueFactory library [36].

The training was conducted over 30 epochs with a batch size of 64, employing the validation losses as the primary criterion for best checkpoint selection and utilizing a learning rate of  $1e - 4$ . The voting scheme and the radius for neighbor searching were optimized on the validation set by AUC scores, which included a single scene for this purpose. During inference, scenes “0015” (comprising approximately 0.4K images) and “0022” (encompassing approximately 0.5K images) from MegaDepth were designated for testing, enabling a focused evaluation of the model performance on these specific subsets.

**Evaluation Metrics.** In the evaluation, we assess the relative poses between the query and the top- $k$  retrieved images using robust estimation techniques. This involves deploying SuperPoint [13] and the state-of-the-art LightGlue [29, 44] for feature detection and matching, followed by OpenCV-RANSAC [17] running for 10K iterations to compute the relative poses. The performance is measured against ground truth (GT) poses by calculating the Area Under the Recall curve (AUC) thresholded at  $10^\circ$  [8, 59], along with the median pose error. The RANSAC threshold is optimized from a set of pixel values  $\{0.5, 1, 2, 3\}$  on the training set. Also, we report the average number of inliers across the retrieved image pairs found by RANSAC. Note that the number of inliers is not an indicator of the accuracy of the estimated pose, as discussed and verified in MQNet [4] and FSNet [5]. In scenarios where  $k > 1$ , for each query, we follow the practical approach and select only the image pair that has the highest number of inliers. This comprehensive evaluation allows us to thoroughly assess the performance not just in retrieving relevant images but also in accurately estimat-

Top →	AUC@10° ↑			Med. pose error (°) ↓			# inliers ↑		
	1	5	10	1	5	10	1	5	10
NetVLAD [2]	56.5	64.2	63.6	2.85	2.36	2.38	234.0	<b>286.5</b>	294.0
CosPlace [6]	54.5	53.5	64.3	3.14	2.34	2.27	<b>239.5</b>	285.0	<b>294.5</b>
CosPlace* [6]	59.3	65.8	<b>66.2</b>	2.58	2.65	<b>2.10</b>	164.0	162.0	255.5
DINov2 [35]	61.1	65.6	64.8	2.32	2.29	2.31	219.0	270.0	282.5
AnyLoc [25]	60.8	65.3	64.1	2.38	2.26	2.35	220.5	273.0	287.5
SALAD [24]	53.9	61.8	62.6	3.23	2.61	2.54	224.5	278.0	285.0
P-NetVLAD [20]	59.7	64.9	64.5	2.67	2.22	2.27	212.5	264.0	283.5
†P-NetVLAD [20]	62.3	64.5	65.1	2.56	2.31	2.21	212.5	262.0	275.5
$R^2$ Former [62]	57.9	65.4	65.7	3.03	2.24	2.21	108.0	185.5	214.0
† $R^2$ Former [62]	<b>64.2</b>	<b>67.9</b>	65.9	<b>2.25</b>	2.05	2.27	186.0	247.0	273.5
<b>VOP</b>	61.8	67.6	66.0	2.36	<b>2.02</b>	2.28	177.5	246.5	251.0

Table 1. Relative pose estimation on MegaDepth using top- $k$  images retrieved by different methods, with the best results in bold at each  $k$  and the overall best underlined. † results are tested using reranking methods prefiltered by the [CLS] tokens from DINov2.

ing their relative poses.

We run hloc [44] on the precomputed matches on top-40 retrieved image pairs and test the poses of the queries using the long-term visual localization benchmark [53]. We compare the percentages of the correctly estimated translations and rotations with errors below  $0.5m$  and  $5^\circ$ , respectively.

Additionally, we visualize some retrieval examples with their baselines and accuracy in Fig. 8 to show the aim of designing retrieval methods tailored for geometric challenges, e.g., pose estimation.

#### 4.1. Pose Estimation on MegaDepth

Table 1 presents the results on the MegaDepth, highlighting the performance of the proposed VOP. The proposed method secures comparable scores for the AUC@10° criterion and exhibits the lowest median pose errors among the SOTA baselines. The underlined results mark the optimal configuration for relative pose accuracy, evidencing the superior performance of the proposed VOP approach when utilizing the top-5 images. This configuration outperforms the global-only retrieval baselines (the first seven rows), reinforcing the significance of selecting correct metrics and model configurations tailored to the specific demands of real-world downstream applications. Our method outperforms the recent reranking approaches  $R^2$ Former [62] and Patch-NetVLAD [20] on MegaDepth when using their pre-trained models. When using the same shortlist we use, their performance (with †) is marginally better than ours. The fine-tuned CosPlace (CosPlace\*) achieves better accuracy than the pretrained model, especially achieving good results on top-10 pairs. Next, we will show the generalization and robustness of the compared methods on unseen data.

#### 4.2. Generalization Experiments

We test the proposed method on multiple real-world scenes from the ETH3D [45] and PhotoTourism [49] datasets for relative pose estimation, and InLoc [51] for localization. We use the model trained on MegaDepth, i.e., no fine-tuning or retraining is done on the following datasets.

**ETH3D** [45] benchmark consists of images with various

Top →	AUC@10° ↑			Med. pose error (°) ↓			# inliers ↑		
	1	5	10	1	5	10	1	5	10
NetVLAD [2]	<b>89.5</b>	90.3	89.9	0.74	0.74	0.79	365.8	147.3	440.1
CosPlace [6]	88.3	89.7	89.7	0.77	0.77	0.78	349.7	<b>426.8</b>	437.2
CosPlace* [6]	43.6	79.7	85.9	38.3	0.79	0.76	62.6	279.0	360.5
DINov2 [35]	87.1	89.2	88.9	<b>0.69</b>	0.67	<b>0.67</b>	338.9	378.2	399.8
AnyLoc [25]	88.9	90.2	90.2	0.76	0.78	0.77	<b>373.2</b>	425.1	438.0
SALAD [24]	89.6	90.2	89.9	0.73	0.76	0.78	385.9	411.2	442.0
P-NetVLAD [20]	86.7	88.4	90.2	0.81	0.83	0.81	333.3	412.4	<b>466.8</b>
†P-NetVLAD [20]	80.5	87.7	89.8	0.87	0.65	0.66	273.2	319.1	355.3
$R^2$ Former [62]	49.1	79.8	90.1	35.2	6.94	0.83	116.5	252.8	364.9
† $R^2$ Former [62]	50.6	81.5	88.2	27.3	0.87	0.80	137.0	318.3	401.5
<b>VOP</b>	83.6	<b>91.1</b>	<b>90.4</b>	<b>0.69</b>	<b>0.61</b>	0.72	293.9	414.7	460.0

Table 2. Relative pose estimation on the ETH3D dataset [45] on the top- $k$  retrieved images using different retrieval methods, with the best results in bold at each  $k$  and the overall best underlined. The proposed VOP is trained on the MegaDepth dataset. † results are tested using reranking methods prefiltered by the [CLS] tokens.

Top →	AUC@10° ↑			Med. pose error (°) ↓			# inliers ↑		
	1	5	10	1	5	10	1	5	10
NetVLAD [2]	55.0	59.3	60.3	3.75	3.10	2.94	283.9	340.0	348.1
CosPlace [6]	53.4	60.8	61.2	3.78	2.91	2.87	<b>291.5</b>	<b>347.0</b>	354.1
CosPlace* [6]	58.3	65.9	66.1	3.59	2.51	2.43	145.9	247.9	281.8
DINov2 [35]	61.1	63.1	63.0	3.17	2.82	2.75	266.0	338.6	<b>356.3</b>
AnyLoc [25]	56.3	60.3	60.6	3.57	2.90	2.81	265.1	334.6	348.6
SALAD [24]	53.5	60.1	59.6	4.07	3.19	3.17	270.7	338.1	349.7
P-NetVLAD [20]	61.9	62.4	61.8	2.76	2.65	2.76	261.9	315.2	339.4
†P-NetVLAD [20]	62.1	63.6	62.8	2.69	2.63	2.71	246.5	322.8	338.5
$R^2$ Former [62]	60.6	<b>67.8</b>	<b>67.9</b>	4.49	2.36	2.35	180.0	241.9	277.6
† $R^2$ Former [62]	<b>63.1</b>	63.9	63.1	2.73	2.55	2.66	216.4	303.5	331.6
<b>VOP</b>	62.5	67.5	65.4	<b>2.63</b>	<b>2.00</b>	<b>2.32</b>	224.5	286.1	281.3

Table 3. Relative pose estimation on the PhotoTourism dataset [49] on the top- $k$  retrieved images using different retrieval methods, with the best results in bold at each  $k$  and the overall best underlined. VOP is trained on the MegaDepth dataset. \* shows fine-tuned Cosplace on Megadepth.

Methods	NetVLAD [2]	Cosplace [6]	Cosplace* [6]	DINov2 [35]	AnyLoc [25]	SALAD [24]	†P-NetVLAD [20]	† $R^2$ Former [62]	<b>VOP</b>
DUC1	65.7	69.2	41.4	63.6	<b>74.7</b>	71.2	60.1	47.0	72.2
DUC2	71.0	74.8	29.0	71.0	75.6	<b>78.6</b>	55.0	66.4	77.1

Table 4. Indoor localization results (recall@5°, 0.5m) on top-40 retrieved image pairs from the InLoc dataset.

viewpoints from *indoor* and *outdoor* scenes, with ground-truth poses reconstructed by laser scanner. 13 scenes are used for testing. All images in the dataset are used as queries to select database images from the rest. Table 2 shows that VOP is always among the top-performing methods. The overall best results in all accuracy metrics are always obtained by VOP by selecting top-5 images. This highlights that VOP performs accurately even without retraining and, thus, is applicable to unseen scenes. The fine-tuned Cosplace does not generalize well to ETH3D, and yields degraded results, especially on the top-1. The reranking methods, P-NetVLAD and  $R^2$ Former, significantly lag behind the performance of VOP, both in their original version and when combined with DINov2 [CLS] tokens.

**PhotoTourism.** Table 3 reports the relative pose estimation results on 11 testing scenes from the PhotoTourism [49] dataset. The proposed VOP achieves the lowest median pose error and the second-best AUC scores. Similar to Tables 1 and 2, Table 3 shows that the number of inliers is not an indicator of accuracy, as we result in fewer inliers while being more accurate than baselines.

**InLoc.** Additionally, we ran all methods on the InLoc

Methods	NetVLAD [2]	Cosplace [6]	Cosplace* [6]	DINOv2 [35]	AnyLoc [25]	SALAD [24]	†P-NetVLAD [20]	†R <sup>2</sup> Former [62]	<b>VOP</b>
Avg. Accuracy (%) ↑	70.1	69.6	56.4	70.5	73.2	72.3	66.2	65.3	<b>75.1</b>
Avg. med. pose error (°) ↓	2.1	2.0	2.0	1.9	2.0	2.2	1.9	1.8	<b>1.5</b>

Table 5. Average accuracy (in percentage) and median pose error (in degrees) on the retrieved top-5 images on the Megadepth [28], ETH3D [45], PhotoTourism [49], and InLoc [51] datasets. InLoc is excluded from the median error, as the official website does not report it. † indicates prefiltering by the [CLS] tokens. \* shows fine-tuned Cosplace on Megadepth. The best results are shown in bold.

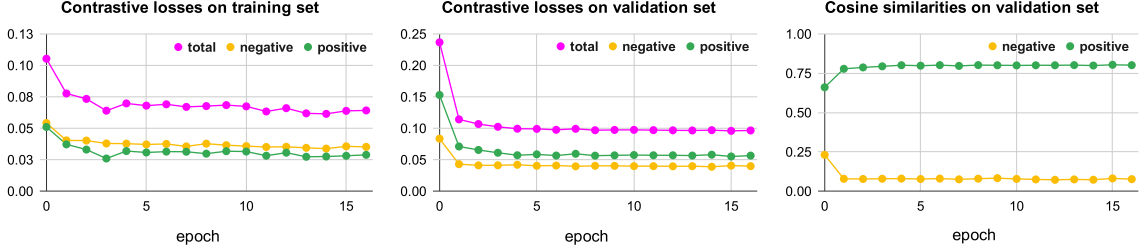


Figure 5. Contrastive losses on the training set (left) and validation (middle) over different epochs shown for negative or positive patch pairs. The right plot shows the average cosine similarities over different patch samples.

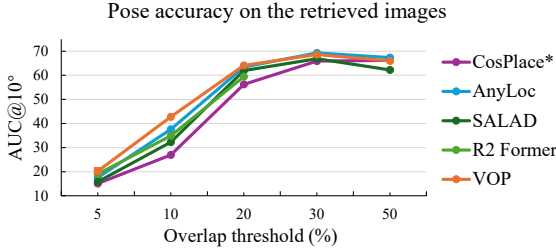


Figure 6. AUC@10° scores on the queries with top-5 images from database images lower than the limits along the horizontal axis.

dataset [51] (without fine-tuning) using hloc [44] for localization to show their generalization capabilities in the case of a large domain gap (in/outdoor). Following hloc [44], we retrieve top-40 database images for all the retrieval methods. For the reranking ones (including VOP), we rerank the top-100 shortlist created by [CLS] token. Table 4 shows the proposed VOP achieves the second highest accuracy, showcasing its generalization abilities. Note that we only show results for P-NetVLAD and R<sup>2</sup>Former with DINOv2 [CLS] token as their original version fails on this dataset.

**In summary**, we show the average accuracy and median pose errors averaged over all tested datasets in Table 5. Note that InLoc is excluded from the median pose error, as the official website does not report it. Overall, the proposed VOP leads to the highest accuracy and lowest pose errors. Fine-tuning Cosplace on Megadepth reduces its accuracy on average, demonstrating that our improved performance is not simply due to the different training data. Again, we do not report results for P-NetVLAD and R<sup>2</sup>Former without DINOv2 [CLS] token due to their failure on InLoc.

### 4.3. Discussions

**Difficult Scenario Experiment.** We conducted an experiment on MegaDepth to retrieve the top-5 images in the

low-overlap scenario. For this test, for each query image, we prefiltered the database by keeping only those images that have a lower overlap with the query than a threshold. Then, we ran image retrieval on this prefiltered database. As shown in Fig. 6, VOP demonstrates clear improvements compared with other methods in this challenging scenario.

**Training.** To better understand the training process, Fig. 5 illustrates the training and validation losses on patch-level contrastive loss and the average similarity changing among different epochs on MegaDepth. It shows the contrastive loss helps to learn the embeddings of negative patches less similar and closer to positive ones, and it converges fast. The similarities shown are averaged over all positive/negative patches of the validation set indicated by the GT labels built from 3D reconstructions.

**Storage & Query Speed.** As we reduce the dimensionality of the DINOv2 features to 256, the embeddings of all patches of each image need a total of 512 kB, while, for AnyLoc, the storage per image is 384 kB. While we require slightly more storage than AnyLoc [25], the difference is small. Compared to storing the local features in the reranking-based methods, VOP costs less. In addition, we compare the time of querying an image from the database of different sizes using AnyLoc or VOP in seconds. Prefiltering top 20 images by DINOv2 [CLS] token and running VOP for reranking to get top-1 out of 500 images cost 0.009 seconds, while 0.003 for AnyLoc. Querying top-1 from 5K images (prefiltered to 100), our method costs 0.03 seconds, while AnyLoc runs in 0.02s. Note that VOP needs much more time for radius search without prefiltering. We recommend using VOP as a reranking method in retrieval.

**Image Patching.** We investigated the number of patches to be used to split the images. The experiments were conducted on the testing scenes of MegaDepth, with all the im-

Patch size	AUC@10° ↑	med. pose err. ↓	recall@5°, 0.5m ↑	
	MegaDepth - top5		DUC1	DUC2
224 <sup>2</sup>	67.0	2.09	30.8	24.4
112 <sup>2</sup>	67.0	2.09	38.4	38.9
56 <sup>2</sup>	66.5	2.17	48.5	57.3
28 <sup>2</sup>	65.9	2.29	59.1	72.5
14 <sup>2</sup>	<b>67.6</b>	<b>2.03</b>	<b>72.2</b>	<b>77.1</b>

Table 6. Ablations on different patch sizes used in inference time. We show the AUC@10° scores and median pose errors of the top-5 retrieved images on MegaDepth [49], and the recall@°, 0.5m on the localization data, Inloc [51] (DUC1, DUC2).

ages resized to 224 × 224. From the trained VOP model with a patch size of 14<sup>2</sup>, we can extract 256 patch descriptors. Then, average pooling is applied to aggregate the patch descriptors to different patch sizes, such as 28<sup>2</sup>, 56<sup>2</sup>, 112<sup>2</sup>, and 224<sup>2</sup>. For example, patch size = 224 will lead to a single patch of an image. The retrieval is done on the same prefiltered image list as discussed. As shown in Table 6, the aggregated patches *e.g.*, patch size=224<sup>2</sup>, perform worse than 14<sup>2</sup> on MegaDepth pose estimation and could not generalize well on Inloc localization. This demonstrates that patch-level features can potentially improve estimated pose and other geometric problems.

**Qualitative Results.** Most VPR methods prioritize retrieving similar images, typically resulting in short baselines that are not suitable for reconstruction. These goals conflict: the most similar images often produce short baselines, making pose estimation unstable. We aim to move beyond traditional similarity metrics and design retrieval methods tailored for geometric challenges, such as selecting images suitable for pose estimation. We visualize three query examples in Fig. 8 with their top-1 retrieved images using different methods. VOP results in low pose errors as we find images with reasonable baselines for stable pose estimation.

## 5. Ablations

We investigate the influence of image patches, different patch sizes, the threshold used in radius search and the influence of the data augmentation on test accuracy and generalization capability.

**Radius Search Threshold.** One of the parameters of the proposed VOP is the radius search threshold when selecting similar patches in the embedding space. To understand how sensitive VOP is to the setting of this threshold, we show tuning results on the validation set of the MegaDepth dataset. We show the results with different thresholds (horizontal axis) on the validation set in Fig. 7. While the accuracy varies with the threshold, setting it on the validation set and using this fixed threshold on *all* tested large-scale datasets leads to SOTA performance. High AUC scores and low pose errors are preferred, thus, threshold = 0.15 is chosen, *i.e.*, the patches with the descriptor similarities lower

Prefilter	Augment	Dropout	AUC@10° ↑	Med. pose error (°) ↓	inliers ↑
✓	×	×	65.1	2.19	<b>272.5</b>
×	✓	×	66.3	2.18	222.0
✓	✓	×	66.7	2.18	263.0
✓	✓	✓	<b>67.6</b>	<b>2.02</b>	246.5

Table 7. Relative pose estimation on the MegaDepth dataset [49] on the top 5 retrieved images using different configurations, with the best results in bold. Prefilter indicates if the [CLS] token was employed to shortlist the potential candidates before overlap prediction. Augment refers to whether data augmentation was used.

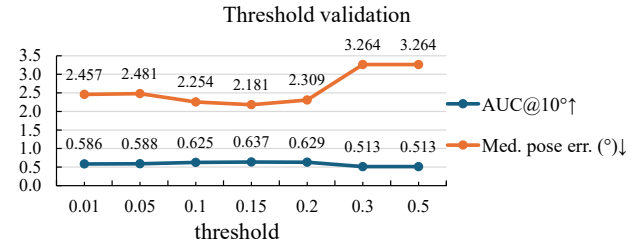


Figure 7. Ablations on the threshold used in radius search. AUC@10° and median pose errors on the validation scene shown.

than 0.15 are recognized as neighbors.

**Dropout Layer.** Table 7 shows the relative pose estimation performance on the top-*k* images retrieved by the model with the searching radius and votings chosen from the best AUC, with or w/o global prefilter ([CLS] tokens), and dropout layer. Testing sets of MegaDepth are used. The CLS prefiltering improves the AUC scores. However, it increases the median pose errors marginally at the same time. As shown in the fifth row, data augmentation is essential in robustly learning the embeddings. Also, the last two rows in Table 7 show that the dropout layer improves the performance on MegaDepth and helps with generalization for pose estimation on other data and indoor localization.

## 6. Conclusion

We introduce a novel Visual Place Recognition method, VOP, focusing on patch-level visual overlap prediction to address challenging viewpoint changes and occlusions. The proposed VOP predicts overlapping image patches by learning a patch-level descriptor and employing a robust voting mechanism and radius search in the descriptor space. Through extensive testing on the MegaDepth, Photo-Tourism, ETH3D, and InLoc datasets, we demonstrate the effectiveness of the proposed VOP. On average, it achieves the highest accuracy, improving upon the state-of-the-art AnyLoc by two AUC points and reducing its median pose error by 25%. We believe this research marks a significant step forward in VPR, breaking the frame of image similarity prediction (through global or local features) to obtain a patch-level understanding of the query and database images.

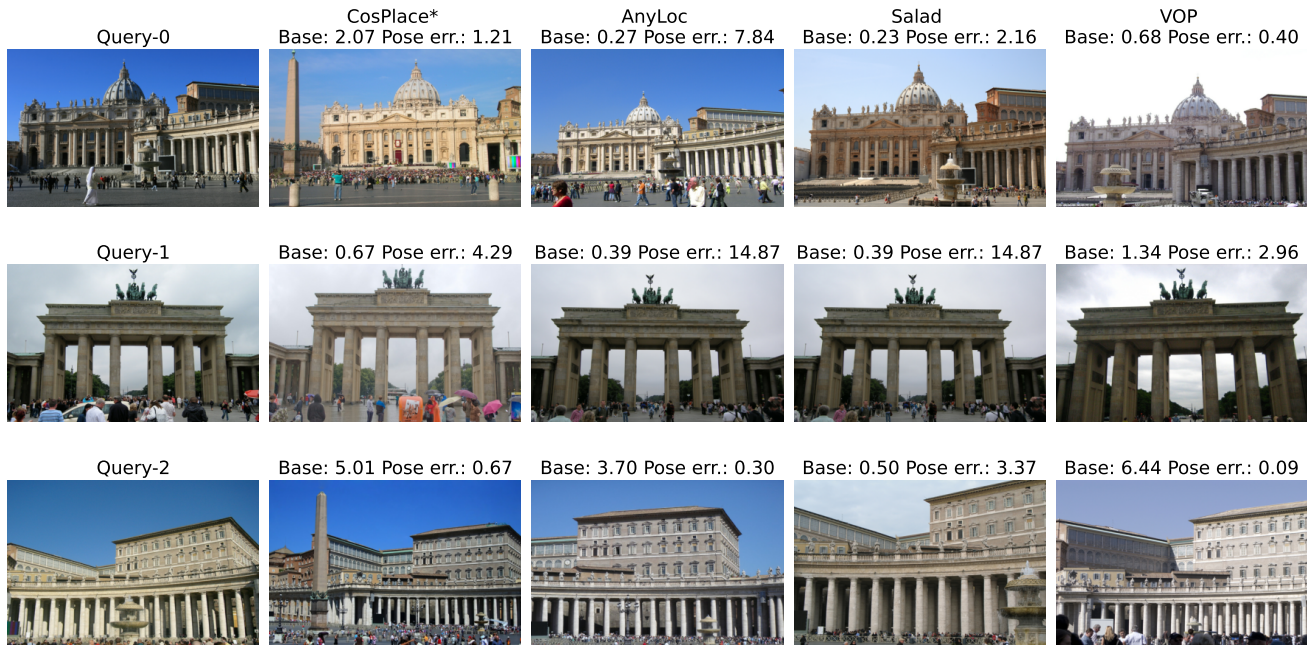


Figure 8. Baselines and pose errors between the retrieved images and queries using different methods shown.

## References

- [1] Amar Ali-bey, Brahim Chaib-draa, and Philippe Giguère. Mixvpr: Feature mixing for visual place recognition. In *WACV*, 2023. 2
- [2] Relja Arandjelovic, Petr Gronat, Akihiko Torii, Tomas Pajdla, and Josef Sivic. NetVLAD: CNN architecture for weakly supervised place recognition. In *CVPR*, 2016. 1, 2, 6, 7, 8
- [3] Relja Arandjelovic and Andrew Zisserman. All about vlad. In *CVPR*, 2013. 3
- [4] Daniel Barath, Luca Cavalli, and Marc Pollefeys. Learning to find good models in ransac. In *Proceedings of the IEEE/CVF Conference on Computer Vision and Pattern Recognition*, 2022. 6
- [5] Axel Barroso-Laguna, Eric Brachmann, Victor Adrian Prisacariu, Gabriel J Brostow, and Daniyar Turmukhambetov. Two-view geometry scoring without correspondences. In *Proceedings of the IEEE/CVF Conference on Computer Vision and Pattern Recognition*, 2023. 6
- [6] Gabriele Berton, Carlo Masone, and Barbara Caputo. Rethinking visual geo-localization for large-scale applications. In *CVPR*, 2022. 1, 2, 6, 7, 8
- [7] Gabriele Berton, Valerio Paolicelli, Carlo Masone, and Barbara Caputo. Adaptive-attentive geolocalization from few queries: A hybrid approach. In *WACV*, 2021. 1, 2
- [8] Eric Brachmann and Carsten Rother. Neural-guided ransac: Learning where to sample model hypotheses. In *ICCV*, 2019. 6
- [9] Carlos Campos, Richard Elvira, Juan J Gómez Rodríguez, José MM Montiel, and Juan D Tardós. Orb-slam3: An accurate open-source library for visual, visual-inertial, and multi-map slam. *IEEE Transactions on Robotics*, 2021. 2
- [10] Zetao Chen, Fabiola Maffra, Inkyu Sa, and Margarita Chli. Only look once, mining distinctive landmarks from convnet for visual place recognition. In *IROS*, 2017. 1
- [11] Gabriella Csurka, Christopher Dance, Lixin Fan, Jutta Willamowski, and Cédric Bray. Visual categorization with bags of keypoints. In *Workshop on statistical learning in computer vision, ECCV*, 2004. 2, 6
- [12] Jonathan Delhumeau, Philippe-Henri Gosselin, Hervé Jégou, and Patrick Pérez. Revisiting the vlad image representation. In *Proceedings of the 21st ACM international conference on Multimedia*, 2013. 1
- [13] Daniel DeTone, Tomasz Malisiewicz, and Andrew Rabinovich. Superpoint: Self-supervised interest point detection and description. In *CVPR Workshops*, 2018. 6
- [14] A.-D. Doan, Y. Latif, T.-J. Chin, Y. Liu, T.-T. Do, and I. Reid. Scalable place recognition under appearance change for autonomous driving. In *ICCV*, 2019. 1
- [15] Anh-Dzung Doan, Yasir Latif, Tat-Jun Chin, Yu Liu, Thanh-Toan Do, and Ian Reid. Scalable place recognition under appearance change for autonomous driving. In *ICCV*, 2019. 1
- [16] Alaaeldin El-Nouby, Natalia Neverova, Ivan Laptev, and Hervé Jégou. Training vision transformers for image retrieval. *arXiv preprint arXiv:2102.05644*, 2021. 2
- [17] Martin A Fischler and Robert C Bolles. Random sample consensus: a paradigm for model fitting with applications to image analysis and automated cartography. *Communications of the ACM*, 1981. 6
- [18] S. Garg, T. Fischer, and M. Milford. Where is your place, visual place recognition? 2021. 2

- [19] S. Garg, N. Suenderhauf, and M. Milford. Semantic-geometric visual place recognition: a new perspective for reconciling opposing views. *The International Journal of Robotics Research*, 2019. 1
- [20] Stephen Hausler, Sourav Garg, Ming Xu, Michael Milford, and Tobias Fischer. Patch-netvlad: Multi-scale fusion of locally-global descriptors for place recognition. In *ICPR*, 2021. 1, 2, 3, 6, 7, 8
- [21] S. Hausler, A. Jacobson, and M. Milford. Multi-process fusion: Visual place recognition using multiple image processing methods. *IEEE Robotics and Automation Letters*, 2019. 1
- [22] Ziyang Hong, Yvan Petillot, David Lane, Yishu Miao, and Sen Wang. Textplace: Visual place recognition and topological localization through reading scene texts. In *ICCV*, 2019. 1
- [23] Sarah Ibrahim, Nanne van Noord, Tim Alpherts, and Marcel Worring. Inside out visual place recognition. In *British Machine Vision Conference*, 2021. 1, 2
- [24] Sergio Izquierdo and Javier Civera. Optimal transport aggregation for visual place recognition. In *CVPR*, 2024. 3, 6, 7, 8
- [25] Nikhil Keetha, Avneesh Mishra, Jay Karhade, Krishna Murthy Jatavallabhula, Sebastian Scherer, Madhava Krishna, and Sourav Garg. Anyloc: Towards universal visual place recognition. *IEEE Robotics and Automation Letters*, 2023. 1, 2, 6, 7, 8
- [26] A. Khaliq, S. Ehsan, Z. Chen, M. Milford, and K. McDonald-Maier. A holistic visual place recognition approach using lightweight cnns for significant viewpoint and appearance changes. *IEEE Transactions on Robotics*, 2020. 1
- [27] Hyo Jin Kim, Enrique Dunn, and Jan-Michael Frahm. Learned contextual feature reweighting for image geolocalization. In *ICPR*, 2017. 2
- [28] Zhengqi Li and Noah Snavely. Megadepth: Learning single-view depth prediction from internet photos. In *CVPR*, 2018. 6, 8
- [29] Philipp Lindenberger, Paul-Edouard Sarlin, and Marc Pollefeys. LightGlue: Local Feature Matching at Light Speed. In *ICCV*, 2023. 4, 5, 6
- [30] Liu Liu, Hongdong Li, and Yuchao Dai. Stochastic attraction-repulsion embedding for large scale image localization. In *ICCV*, 2019. 1
- [31] David G. Lowe. Distinctive image features from scale-invariant keypoints. *IJCV*, 2004. 2
- [32] Ivan Moskalenko, Anastasiia Kornilova, and Gonzalo Ferrer. Visual place recognition for aerial imagery: A survey. *arXiv preprint arXiv:2406.00885*, 2024. 1
- [33] Raul Mur-Artal, Jose Maria Martinez Montiel, and Juan D Tardos. Orb-slam: a versatile and accurate monocular slam system. *IEEE transactions on robotics*, 2015. 2
- [34] Raul Mur-Artal and Juan D Tardós. Orb-slam2: An open-source slam system for monocular, stereo, and rgb-d cameras. *IEEE transactions on robotics*, 2017. 2
- [35] Maxime Oquab, Timothée Darcet, Théo Moutakanni, Huy Vo, Marc Szafraniec, Vasil Khalidov, Pierre Fernandez, Daniel Haziza, Francisco Massa, Alaaeldin El-Nouby, et al. Dinov2: Learning robust visual features without supervision. *arXiv preprint arXiv:2304.07193*, 2023. 3, 4, 5, 7, 8
- [36] Rémi Pautrat\*, Iago Suárez\*, Yifan Yu, Marc Pollefeys, and Viktor Larsson. GlueStick: Robust Image Matching by Sticking Points and Lines Together. In *ICCV*, 2023. 6
- [37] Guohao Peng, Yufeng Yue, Jun Zhang, Zhenyu Wu, Xiaoyu Tang, and Danwei Wang. Semantic reinforced attention learning for visual place recognition. In *ICRA*, 2021. 2
- [38] Guohao Peng, Jun Zhang, Heshan Li, and Danwei Wang. Attentional pyramid pooling of salient visual residuals for place recognition. In *ICCV*, 2021. 2
- [39] James Philbin, Ondrej Chum, Michael Isard, Josef Sivic, and Andrew Zisserman. Object retrieval with large vocabularies and fast spatial matching. In *CVPR*, 2007. 2
- [40] Filip Radenović, Giorgos Tolias, and Ondřej Chum. Fine-tuning cnn image retrieval with no human annotation. *IPAMI*, 2018. 2
- [41] Juan Ramos et al. Using tf-idf to determine word relevance in document queries. In *Proceedings of the first instructional conference on machine learning*, 2003. 6
- [42] Jerome Revaud, Jon Almazán, Rafael S Rezende, and Cesar Roberto de Souza. Learning with average precision: Training image retrieval with a listwise loss. In *ICCV*, 2019. 2
- [43] Pedro OCS Ribeiro, Matheus M dos Santos, Paulo LJ Drews, Silvia SC Botelho, Lucas M Longaray, Giovanni G Giacomo, and Marcelo R Pias. Underwater place recognition in unknown environments with triplet based acoustic image retrieval. In *ICMLA. IEEE*, 2018. 1
- [44] Paul-Edouard Sarlin, Cesar Cadena, Roland Siegwart, and Marcin Dymczyk. From coarse to fine: Robust hierarchical localization at large scale. In *CVPR*, 2019. 6, 7, 8
- [45] Thomas Schops, Johannes L Schonberger, Silvano Galliani, Torsten Sattler, Konrad Schindler, Marc Pollefeys, and Andreas Geiger. A multi-view stereo benchmark with high-resolution images and multi-camera videos. In *CVPR*, pages 3260–3269, 2017. 6, 7, 8
- [46] Shihao Shao, Kaifeng Chen, Arjun Karpur, Qinghua Cui, André Araujo, and Bingyi Cao. Global features are all you need for image retrieval and reranking. In *ICCV*, 2023. 3
- [47] Ali Sharif Razavian, Hossein Azizpour, Josephine Sullivan, and Stefan Carlsson. Cnn features off-the-shelf: an astounding baseline for recognition. In *CVPR workshops*, 2014. 3
- [48] Sivic and Zisserman. Video google: A text retrieval approach to object matching in videos. In *ICCV. IEEE*, 2003. 2
- [49] Noah Snavely, Steven M Seitz, and Richard Szeliski. Photo tourism: exploring photo collections in 3D. In *SIGGRAPH*. 2006. 6, 7, 8
- [50] Arulkumar Subramaniam, Prashanth Balasubramanian, and Anurag Mittal. Ncc-net: Normalized cross correlation based deep matcher with robustness to illumination variations. In *WACV. IEEE*, 2018. 1
- [51] Hajime Taira, Masatoshi Okutomi, Torsten Sattler, Mircea Cimpoi, Marc Pollefeys, Josef Sivic, Tomas Pajdla, and Akihiko Torii. Inloc: Indoor visual localization with dense matching and view synthesis. In *CVPR*, 2018. 6, 7, 8

- [52] Fuwen Tan, Jiangbo Yuan, and Vicente Ordonez. Instance-level image retrieval using reranking transformers. In *ICCV*, 2021. [3](#)
- [53] Carl Toft, Will Maddern, Akihiko Torii, Lars Hammarstrand, Erik Stenborg, Daniel Safari, Masatoshi Okutomi, Marc Pollefeys, Josef Sivic, Tomas Pajdla, et al. Long-term visual localization revisited. *TPAMI*, 2020. [7](#)
- [54] Giorgos Tolias, Yannis Avrithis, and Hervé Jégou. Image search with selective match kernels: aggregation across single and multiple images. *IJCV*, 2016. [2](#)
- [55] A. Torii, R. Arandjelovic, J. Sivic, M. Okutomi, and T. Pajdla. 24/7 place recognition by view synthesis. *IEEE Transactions on Pattern Analysis and Machine Intelligence*, 2018. [1](#)
- [56] A. Torii, Hajime Taira, Josef Sivic, M. Pollefeys, M. Okutomi, T. Pajdla, and Torsten Sattler. Are large-scale 3d models really necessary for accurate visual localization? *TPAMI*, 2021. [1](#)
- [57] Ruotong Wang, Yanqing Shen, Weiliang Zuo, Sanping Zhou, and Nanning Zheng. TransVPR: Transformer-based place recognition with multi-level attention aggregation. In *CVPR*, 2022. [3](#)
- [58] Frederik Warburg, Soren Hauberg, Manuel Lopez-Antequera, Pau Gargallo, Yubin Kuang, and Javier Civera. Mapillary street-level sequences: A dataset for lifelong place recognition. In *CVPR*, 2020. [1](#), [2](#)
- [59] Kwang Moo Yi\*, Eduard Trulls\*, Yuki Ono, Vincent Lepetit, Mathieu Salzmann, and Pascal Fua. Learning to find good correspondences. In *CVPR*, 2018. [6](#)
- [60] M. Zaffar, S. Garg, M. Milford, et al. Vpr-bench: An open-source visual place recognition evaluation framework with quantifiable viewpoint and appearance change. *IJCV*, 2021. [1](#)
- [61] Liang Zheng, Yi Yang, and Qi Tian. Sift meets cnn: A decade survey of instance retrieval. *TPAMI*, 2017. [2](#)
- [62] Sijie Zhu, Linjie Yang, Chen Chen, Mubarak Shah, Xiaohui Shen, and Heng Wang. R2former: Unified retrieval and reranking transformer for place recognition. In *CVPR*, 2023. [2](#), [3](#), [6](#), [7](#), [8](#)